LETTERS
PUBLISHED ONLINE: 25 APRIL 2016 | DOI: 10.1038/NCLIMATE2996
nature climate change

Pacific trade winds accelerated by aerosol forcing over the past two decades

Chiharu Takahashi and Masahiro Watanabe*

The Pacific trade winds, coupled with the zonal sea surface temperature gradient in the equatorial Pacific Ocean, control regional sea levels[1], and therefore their trend is a great concern in the Pacific Rim. Over the past two decades, easterly winds have been accelerated in association with eastern tropical Pacific cooling[2]. They may represent natural interdecadal variability in the Pacific[3] and possibly explain the recent global warming hiatus[4–7]. However, the intensification of the winds has been the strongest ever observed in the past century[2,5,8], the reason for which is still unclear. Here we show, using multiple climate simulations for 1921–2014 by a global climate model, that approximately one-third of the trade-wind intensification for 1991–2010 can be attributed to changes in sulfate aerosols. The multidecadal sea surface temperature anomaly induced mostly by volcanic aerosols dominates in the western North Pacific, and its sign changed rapidly from negative to positive in the 1990s, coherently with Atlantic multidecadal variability[9–11]. The western North Pacific warming resulted in intensification of trade winds to the west of the dateline. These trends have not contributed much to the global warming hiatus, but have greatly impacted rainfall over the western Pacific islands.

Changes in the tropical Pacific sea surface temperature (SST) and surface winds over the past two decades, namely, La Niña-like cooling in the eastern Pacific and intensified surface easterly winds, are important for understanding the recent pause of global-mean surface temperature increase called the warming hiatus[4–6]. The La Niña-like SST anomalies act to prevent the global surface temperature from rising via teleconnection[4], and accelerated trade winds enhance ocean heat uptake, which suppresses surface warming[5,12,13]. Although most of these decadal-scale changes in SSTs and winds fit well with the negative phase of the Interdecadal Pacific Oscillation (IPO), a dominant natural variability on interannual-to-interdecadal timescales in the Pacific[3,14], the marked intensification of trade winds during 1992–2011 may not be explained by the IPO alone[5].

Intensification of trade winds over the past two decades has occurred despite a longer-term weakening trend, which is plausibly a response of the Walker circulation to global warming[15,16]. The magnitude of the trade winds can be altered either by cooling of the eastern basin or warming of the western basin, making it difficult to attribute the trade-wind changes to external forcing. The Coupled Model Intercomparison Project Phase 5 (CMIP5) simulations for the twentieth and twenty-first centuries show that externally forced SST changes appear strongly in the western Pacific[17,18], so that the external driving of the Pacific trade winds may occur through changes in the warm pool SST.

Historical changes in well-mixed greenhouse gases show a monotonic increase, which was unlikely to have caused the decadal variability of SST and associated surface winds. Among other external radiative forcings, natural volcanic and anthropogenic sulfate aerosols have been shown to drive multidecadal changes in the North Atlantic SST[19], the frequency of Atlantic hurricanes[20], the North Pacific SST[21], and the south Asian summer monsoon[22]. Because sulfate aerosols injected into the atmosphere act to cool the Earth's surface by scattering or absorbing solar radiation, as well as by interacting with clouds[23], a series of large eruptions and a peak in anthropogenic emissions from North America and Europe, occurring concurrently between the 1960s and early 1990s (Supplementary Fig. 1), could have caused a cooler climate during this period. However, there is a critique to the aerosol forcing of the North Atlantic SST variability[24]; furthermore, aerosol-induced multidecadal anomalies have not been identified in the tropical Pacific so far.

Here, we first demonstrate that sulfate aerosol forcing was critical for the multidecadal SST variability in the tropical western Pacific and contributed to the intensification of the Pacific trade winds over the past two decades. The above results are based on a five-member ensemble climate simulation for 1921–2014 using a state-of-the-art atmosphere–ocean coupled general circulation model (CGCM) called MIROC5.2 (ref. 6; see Methods). In addition to the historical simulation driven by all external forcing agents (denoted as HIST), we performed two modified historical experiments in which either volcanic or both volcanic and anthropogenic sulfate aerosols were prescribed to their pre-industrial levels (VOLCONST and SO2CONST, respectively). A combined analysis of the three sets of experiments, 15 ensembles altogether, enables us to quantitatively estimate the contributions of anthropogenic and volcanic sulfate aerosols to the trends in the SST and trade winds for 1991–2010.

Empirical orthogonal functions (EOFs) to detrended 10-year low-pass-filtered SST anomalies (called decadal SST anomalies, see Methods) over the tropical Pacific (25° S–25° N and 100° E–80° W) were used to extract two dominant patterns of variability in the observations (Fig. 1a,b). The first EOF (EOF1) shows a pattern similar to the IPO, having its maximum amplitudes in the central-eastern equatorial Pacific and the North Pacific with opposite signs (Fig. 1a). The second EOF (EOF2) exhibits a prominent warming pattern extending from the equatorial western Pacific into the extratropical Pacific, and accompanies significant warming signals in the Atlantic and the eastern Indian oceans (Fig. 1b). A pattern of sea-level pressure (SLP) anomalies associated with EOF2 reveals a tropics-wide dipole between the eastern and western hemispheres (Supplementary Fig. 2). This variability represents a modulation of the entire Walker circulation linking tropical ocean basins, and is therefore referred to as the trans-basin variability (TBV)[9,10].

The above two dominant modes are obtained from HIST as well, showing that the overall patterns are in good agreement with observations (Fig. 1c,d). Characteristics of the principal component

Atmosphere and Ocean Research Institute, The University of Tokyo, 5-1-5 Kashiwanoha, Kashiwa, Chiba 277-8568, Japan. *e-mail: hiro@aori.u-tokyo.ac.jp

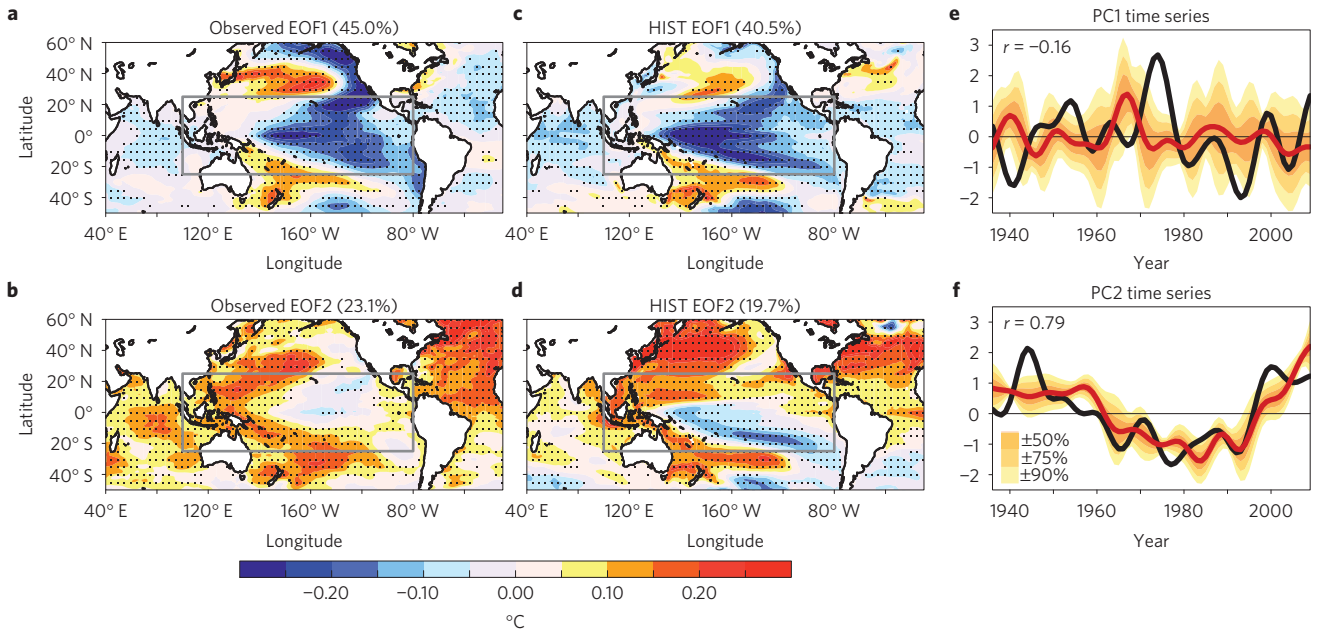

Figure 1 | Two dominant decadal SST patterns and time series for 1936–2009. a,**b**, Observed low-frequency detrended SST anomalies regressed on the PCs associated with EOF1 and EOF2, respectively, to the tropical Pacific SST (grey rectangles). The fractional variance is denoted at the top. Stippling indicates regions exceeding the 95% statistical significance. **c**,**d**, As in **a**,**b**, but for the HIST five-member ensemble. **e**,**f**, Corresponding PC time series for observations (black) and simulations (red curve for the ensemble mean and shading for the ensemble spread). Correlation coefficients between the observed and simulated PC time series are shown.

Table 1 | Fractional contributions of external radiative forcing to SST trends in the WNP and tropical Atlantic for 1991–2010.

Region	SST trend (°C per decade)		Fractional contribution (%)		
	COBE SST	HIST	Anthropogenic SO_2	Volcanic SO_2	Others (GHGs and so on)
WNP	0.27 ± 0.21	0.23 ± 0.12	−22	89	33
Tropical Atlantic	0.21 ± 0.15	0.21 ± 0.11	29	73	−2

Contributions (%) of anthropogenic sulfate aerosols, natural volcanic sulfate aerosols and other radiative forcing factors including greenhouse gases (GHGs) to the SST trends that were estimated by using HIST, SO2CONST and VOLCONST (see Methods). The SST trends (°C) for observations (COBE SST)[31] and the HIST ensemble mean (with the uncertainty ranges, see Methods) are also indicated. The WNP and tropical Atlantic regions are defined in Fig. 2a.

(PC) time series associated with the two simulated EOFs reveal their different origins. The PC1 time series shows a large spread, which represents the different phases and amplitudes of decadal variability across ensemble members, and the ensemble-mean values are weak and negatively correlated with the observed PC1 scores (Fig. 1e). Although the interannual variability associated with the El Niño–La Niña cycle is not fully filtered out, the observed PC1 exhibits a positive decadal trend beginning in the early 1990s. In contrast, the PC2 time series representing the TBV shows multidecadal changes (positive before the 1960s and after the mid-1990s, and negative between them) both in the observations and HIST (Fig. 1f). Unlike EOF1, the spread of PC2 is small, and the ensemble-mean time series is highly correlated with the observations ($r = 0.79$). Additional EOF analyses of the HIST ensemble mean and ensemble deviations strengthen our interpretation that the IPO represents natural variability intrinsic to the Pacific atmosphere–ocean system, whereas the TBV represents the externally forced variability (Supplementary Fig. 3). In the western subtropical North/South Pacific and the North Atlantic, where TBV-related SST anomalies dominate (Fig. 1b), the observed decadal/interdecadal SST variability is reproduced well by the ensemble-mean anomalies in HIST (Fig. 2a). We focus on the western North Pacific (WNP) region of 130°–180° E and 10°–25° N (red box in Fig. 2a), because the decadal variability in this area is the least affected by the IPO, but is rather controlled by the TBV (Fig. 1a,b). Indeed, the time series of WNP SST anomalies exhibits multidecadal variability similar to PC2 both in observations and HIST (Fig. 2b,c). In the mid-1990s, the WNP SST anomalies rapidly changed their sign from negative to positive, resulting in 1991–2010 warming trends of 0.27 ± 0.21 and 0.23 ± 0.12 °C per decade in the observations and HIST, respectively. Interestingly, the ensemble-mean SST anomalies in SO2CONST are unable to reproduce most of the multidecadal changes, with a negligible and insignificant linear trend for 1991–2010 (0.08 ± 0.05 °C per decade) (Fig. 2d). This provides clear modelling evidence that multidecadal SST variability in the WNP region has been driven by past changes in sulfate aerosols.

Observed SST trends for 1991–2010 show similar values in the WNP and tropical Atlantic (red and blue box regions in Fig. 2a). As most of these trends have been induced by sulfate aerosols (Fig. 2 and Supplementary Fig. 4), the relative contributions of anthropogenic and volcanic sulfate aerosols to the simulated SST trends can be estimated (see Methods). It has been identified that volcanic aerosols have predominantly contributed to the warming in both regions (Table 1). Actually, the sulfate aerosol radiative effect is negative, and therefore this volcanic forcing for 1991–2010 is interpreted as a recovery from the Pinatubo-induced cooling period in the early 1990s[25,26] (Fig. 2c). In the tropical Atlantic,

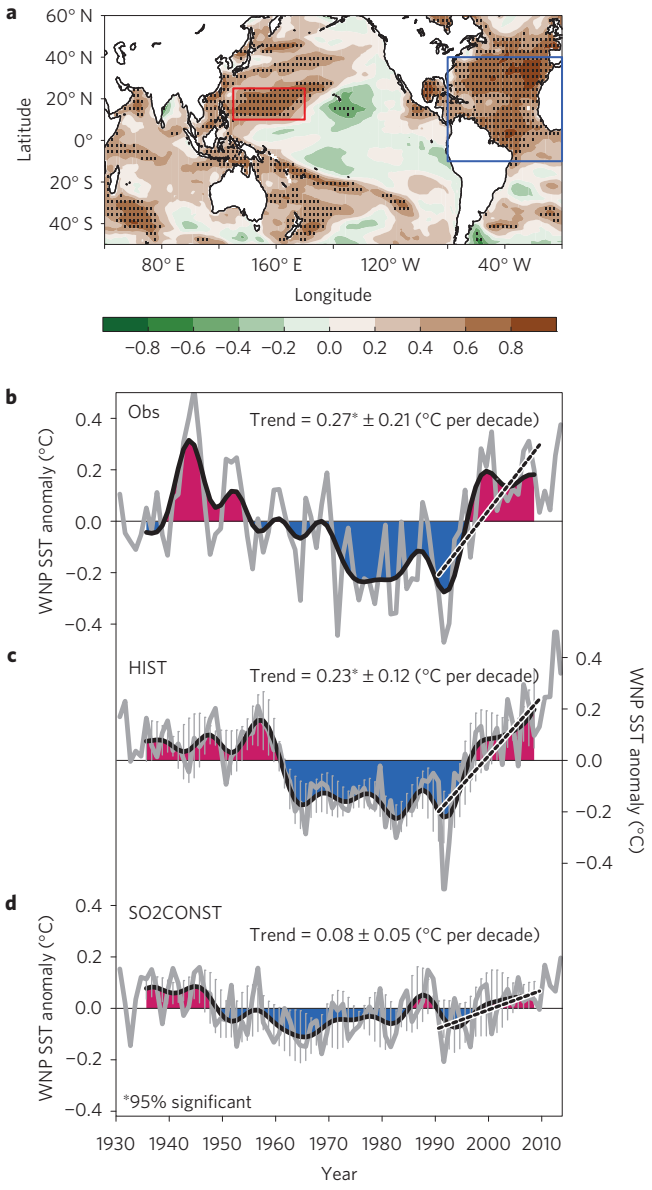

Figure 2 | Multidecadal SST variability in the WNP for 1931–2014. a, Local correlation map for the low-frequency SST anomalies between observations and the HIST ensemble mean. Stippling indicates regions exceeding the 95% statistical significance. **b**–**d**, Time series of detrended annual-mean SST anomalies (bold grey curve) and their low-frequency components (black curve with shading) averaged in the WNP (red rectangle in **a**) in observations, HIST and SO2CONST, respectively. The thick black curves and thin grey bars in **c**,**d**, indicate the ensemble mean and the spread. Linear trends for 1991–2010 are shown by dashed black lines.

decline of anthropogenic aerosols also contributed to the warming trend by about 30%, consistent with a previous model experiment[19]. However, the anthropogenic sulfate aerosols counteract the effect of volcanic aerosols in the WNP. This may be reasonable, given the continuous increase of anthropogenic emissions over Asia (Supplementary Fig. 1).

As the volcanic impact on SST tends to disappear within five years[26], it cannot explain the WNP warming after the late 1990s (Fig. 2). Another possible driver for multidecadal SST variability in the WNP is large-scale atmosphere–ocean dynamics coupled with aerosol forcing[27]. Unlike the Atlantic Ocean, where direct and indirect aerosol effects work together to generate the multidecadal SST variability (Supplementary Fig. 5), the net aerosol forcing to the WNP SST variability is weak, and instead decadal change in the surface latent heat flux generates the SST variability (Supplementary Fig. 6). The contrast of surface energy budgets between the WNP and tropical Atlantic suggests that the latter region is the major source of the TBV, consistent with arguments in previous studies[9–11]. This remote mechanism working with dominant volcanic aerosol forcing can explain why the WNP SST anomalies show a significant warming trend during 1991–2010.

The observed SST trends for 1991–2010 show cooling in the eastern tropical Pacific but warming in the western Pacific and Indian Ocean, accompanied by increased rainfall over the Maritime Continent and decreased rainfall over the central equatorial Pacific (Fig. 3a). The greater zonal contrasts in SST and precipitation link to the intensification of the Pacific trade winds (Fig. 3c). Decomposition of the SST trend pattern using two EOFs clearly shows that the warming in the western Pacific is attributable to the positive trend in the TBV (Supplementary Fig. 7), which is captured by the HIST ensemble mean (Fig. 3b). In the model, increasing zonal contrasts in SST and precipitation are confined to the region west of the dateline. The HIST ensemble mean reproduces neither eastern Pacific cooling trends nor the warming hiatus in global-mean surface temperature (Supplementary Fig. 8), consistent with the argument that the warming hiatus is largely induced by internal climate variability[6,7]. Yet, the Pacific trade winds were intensified in the HIST ensemble-mean fields (Fig. 3d). The accelerated surface easterlies promote the accumulation of ocean subsurface water and raise sea levels in the western Pacific[28,29], so that salient features of the observed increasing trend in the 0–300 m heat content (HC_{300}) are captured by the HIST ensemble mean (Fig. 3c,d).

The Pacific trade-wind anomaly associated with the TBV is measured by the surface zonal wind averaged over 5° S–5° N and 140° E–170° W (yellow box in Fig. 3c,d). The observed trade-wind index calculated with two independent reanalysis data sets (Methods) shows the decadal variability imposed on a multidecadal change, which has a significant negative trend during 1991–2010 (Fig. 4a). Evaluation of the 20-year linear trends with a sliding window shows that the above trend was never observed over the previous eight decades, and that it is associated with pronounced increasing trends in the WNP SST and the western Pacific HC_{300} anomalies (Fig. 4d).

Although the magnitude is smaller than the observations, ensemble-mean anomalies in HIST show trade-wind intensification and associated increases in the WNP SST and western Pacific HC_{300} after the 1990s (Fig. 4b,e). The simulated zonal wind trend for 1991–2010 is $-0.28 \pm 0.12\,m\,s^{-1}$ per decade, which accounts for $34 \pm 18\%$ of the observed trends. It is clear from the comparison of the trends between HIST and SO2CONST that the intensification of the trade winds in the HIST ensemble mean was induced by sulfate aerosol forcing (Fig. 4b,c,e,f). The discrepancy in magnitude between the observations and HIST is large, and could be attributed to the negative IPO and the influence of Indian Ocean warming[29,30]. As the simulated internal variability of trade winds appears weaker than observations (Fig. 4a,b), the uncertainty range of the forced trend might actually be larger. Nevertheless, the influence of sulfate aerosols is robust, without which the Pacific trade winds would not have reached record levels of intensification during 1991–2010.

An indication of external driving for the multidecadal changes in the WNP SST is also obtained from the CMIP5 multi-model ensemble, which reproduces the multidecadal SST variability in the WNP and tropical Atlantic, as well as intensification of trade winds (Supplementary Fig. 9). Although aerosol forcing cannot explain a part of the trade-wind intensification responsible for the global warming hiatus[4–6] (Supplementary Fig. 8), our findings are relevant for understanding decadal climate changes in the Pacific. If sulfate aerosol cooling is strengthened again in the near future by large

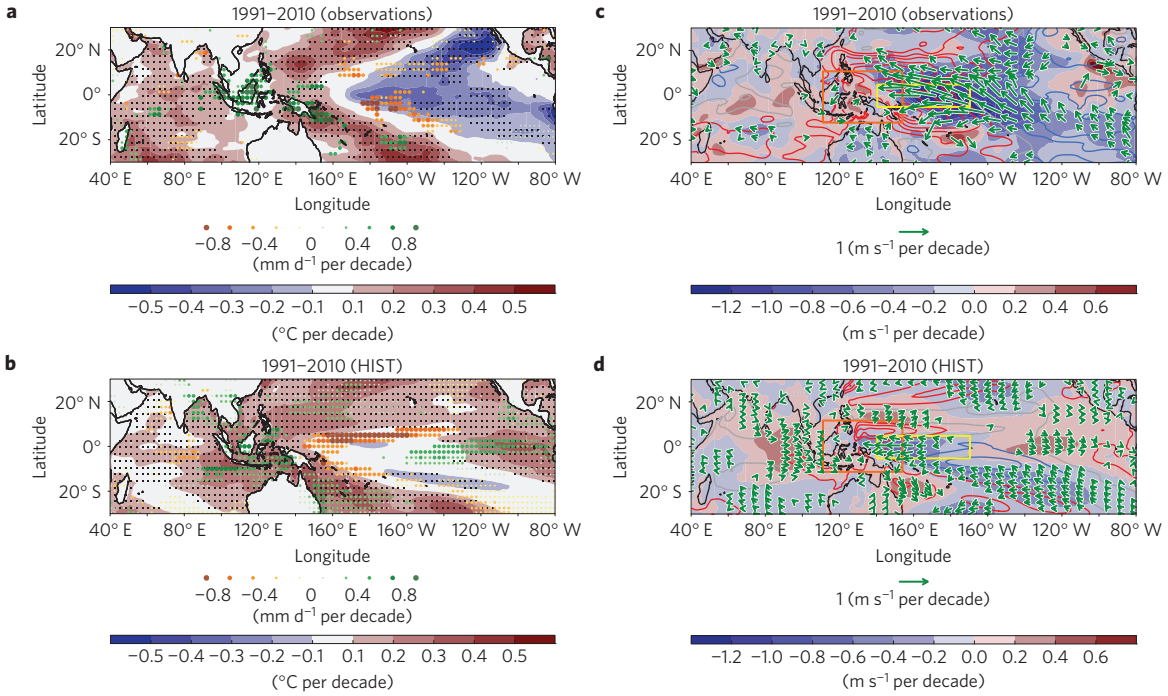

Figure 3 | Observed and simulated trends during 1991–2010. a,**b**, Trends in SST (shading) and precipitation (circles) anomalies from observations and the HIST ensemble mean. Stippling indicates regions exceeding the 95% statistical significance. **c**,**d**, As in **a**,**b**, but for surface zonal wind (shading), HC_{300} (contour, red for positive and blue for negative values, in unit of 10^{19} J m^2 per decade, interval ±0.2, 0.4, 0.6, 0.9, 1.2), and surface wind anomalies (green arrows). The yellow and orange boxes represent the areas of zonal wind and HC_{300} presented in Fig. 4. The wind vectors significant at the 95% level are plotted.

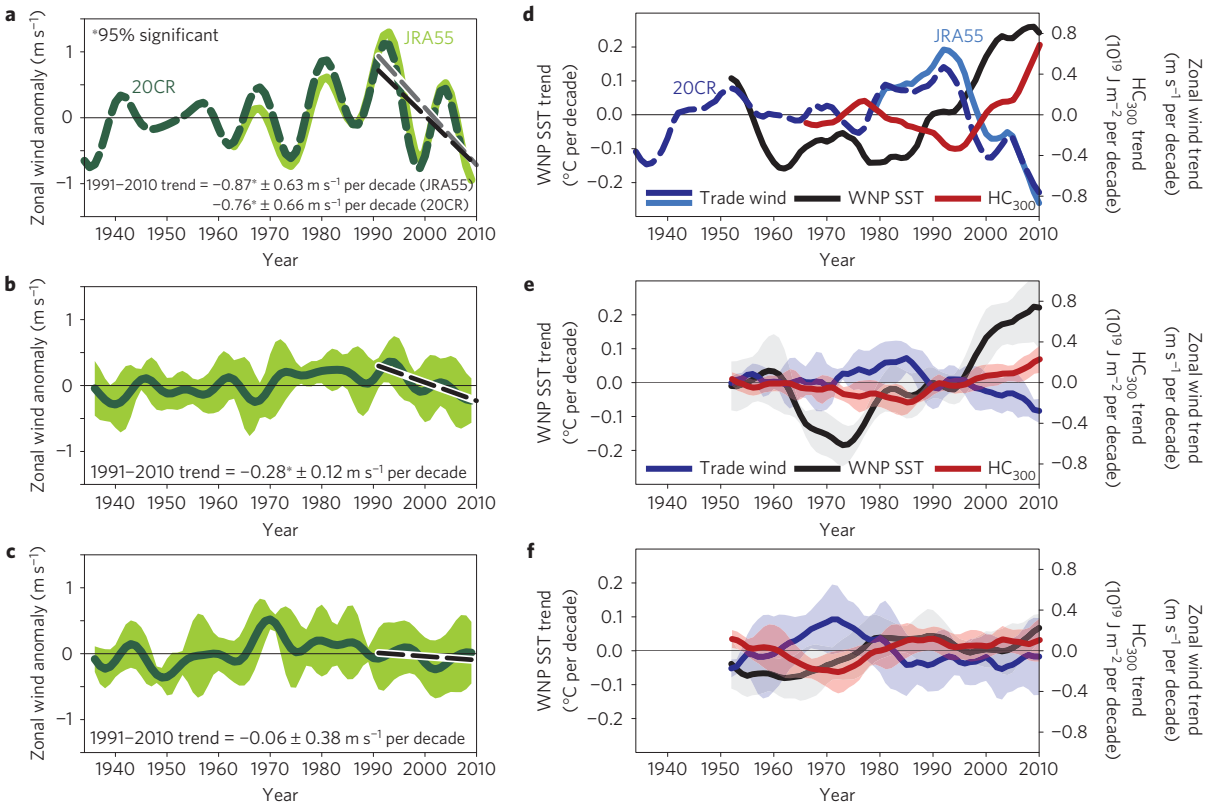

Figure 4 | Twenty-year trends in the Pacific trade winds and associated ocean anomalies for 1935–2010. a–**c**, Time series of the Pacific trade-wind index (defined in Fig. 3) from two reanalysis data sets (**a**), HIST (**b**) and SO2CONST (**c**) (thick curves and the shading indicate the ensemble mean and spread). Linear trends for 1991–2010 are also presented. **d**–**f**, As in **a**–**c**, but for 20-year trends with a sliding window, leading up to each year shown, for the WNP SST, Pacific trade-wind index, and western Pacific HC_{300}.

volcanic eruptions or further increases of anthropogenic emissions from Asia, it could cause regional sea-level rises and enhanced drying over the Maritime Continents, both of which would seriously impact the Pacific islands.

Methods

Methods and any associated references are available in the online version of the paper.

Received 15 December 2015; accepted 18 March 2016; published online 25 April 2016

References

1. Merrifield, M. A. A shift in western tropical Pacific sea level trends during the 1990s. *J. Clim.* **24,** 4126–4138 (2011).
2. L'Heureux, M. L., Lee, S. & Lyon, B. Recent multidecadal strengthening of the Walker circulation across the tropical Pacific. *Nature Clim. Change* **3,** 571–576 (2013).
3. Meehl, G. A., Hu, A., Arblaster, J. M., Fasullo, J. Y. & Trenberth, K. E. Externally forced and internally generated decadal climate variability associated with the Interdecadal Pacific Oscillation. *J. Clim.* **26,** 7298–7310 (2013).
4. Kosaka, Y. & Xie, S.-P. Recent global-warming hiatus tied to equatorial Pacific surface cooling. *Nature* **501,** 403–407 (2013).
5. England, M. H. *et al*. Recent intensification of wind-driven circulation in the Pacific and the ongoing warming hiatus. *Nature Clim. Change* **4,** 222–227 (2014).
6. Watanabe, M. *et al*. Contribution of natural decadal variability to global warming acceleration and hiatus. *Nature Clim. Change* **4,** 893–897 (2014).
7. Dai, A., Fyfe, J. C., Xie, S.-P. & Dai, X. Decadal modulation of global surface temperature by internal climate variability. *Nature Clim. Change* **5,** 555–560 (2015).
8. de Boisséson, E., Balmaseda, M. A., Abdalla, S., Källén, E. & Janssen, P. A. E. M. How robust is the recent strengthening of the tropical Pacific trade winds? *Geophys. Res. Lett.* **41,** 4398–4405 (2014).
9. McGregor, S. *et al*. Recent Walker circulation strengthening and Pacific cooling amplified by Atlantic warming. *Nature Clim. Change* **4,** 888–892 (2014).
10. Chikamoto, Y. *et al*. Skillful multi-year predictions of tropical trans-basin climate variability. *Nature Commun.* **6,** 6869 (2015).
11. Li, X., Xie, S.-P., Gille, S. T. & Yoo, C. Atlantic-induced pan-tropical climate change over the past three decades. *Nature Clim. Change* **6,** 275–279 (2015).
12. Watanabe, M. *et al*. Strengthening of ocean heat uptake efficiency associated with the recent climate hiatus. *Geophys. Res. Lett.* **40,** 3175–3179 (2013).
13. Drijfhout, S. S. *et al*. Surface warming hiatus caused by increased heat uptake across multiple ocean basins. *Geophys. Res. Lett.* **41,** 7868–7874 (2014).
14. Power, S., Casey, T., Folland, C., Colman, A. & Mehta, V. Interdecadal modulation of the impact of ENSO on Australia. *Clim. Dynam.* **15,** 319–324 (1999).
15. Vecchi, G. A. *et al*. Weakening of tropical Pacific atmospheric circulation due to anthropogenic forcing. *Nature* **441,** 73–76 (2006).
16. Held, I. M. & Soden, B. J. Robust responses of the hydrological cycle to global warming. *J. Clim.* **19,** 5686–5699 (2006).
17. Boer, G. J. Decadal potential predictability of twenty-first century climate. *Clim. Dynam.* **36,** 1119–1133 (2011).
18. Funk, C. C. & Hoell, A. The leading mode of observed CMIP5 ENSO-residual sea surface temperatures and associated changes in Indo-Pacific climate. *J. Clim.* **28,** 4309–4329 (2015).
19. Booth, B. B. B., Dunstone, N. J., Halloran, P. R., Andrews, T. & Bellouin, N. Aerosols implicated as a prime driver of twentieth-century North Atlantic climate variability. *Nature* **484,** 228–232 (2012).
20. Dunstone, N. J., Smith, D. M., Booth, B. B. B., Hermanson, L. & Eade, R. Anthropogenic aerosol forcing of Atlantic tropical storms. *Nature Geosci.* **6,** 534–539 (2013).
21. Boo, K.-O. *et al*. Influence of aerosols in multidecadal SST variability simulations over the North Pacific. *J. Geophys. Res.* **120,** 517–531 (2015).
22. Bollasina, M. A., Ming, Y. & Ramaswamy, V. Anthropogenic aerosols and the weakening of the South Asian summer monsoon. *Science* **334,** 502–505 (2011).
23. Lohmann, U. & Feichter, J. Global indirect aerosol effects: a review. *Atmos. Chem. Phys.* **5,** 715–737 (2005).
24. Zhang, R. *et al*. Have aerosols caused the observed Atlantic multidecadal variability? *J. Atmos. Sci.* **70,** 1135–1144 (2013).
25. Santer, B. D. *et al*. Volcanic contribution to decadal changes in tropospheric temperature. *Nature Geosci.* **7,** 185–189 (2014).
26. Maher, N., McGregor, S., England, M. H. & Gupta, A. S. Effects of volcanism on tropical variability. *Geophys. Res. Lett.* **42,** 6024–6033 (2015).
27. Xie, S.-P., Lu, B. & Xiang, B. Similar spatial patterns of climate responses to aerosol and greenhouse gas changes. *Nature Geosci.* **6,** 828–832 (2013).
28. Merrifield, M. A. & Maltrud, M. E. Regional sea level trends due to a Pacific trade wind intensification. *Geophys. Res. Lett.* **38,** L21605 (2011).
29. Han, W. *et al*. Intensification of decadal and multi-decadal sea level variability in the western tropical Pacific during recent decades. *Clim. Dynam.* **43,** 1357–1379 (2014).
30. Luo, J. J., Sasaki, W. & Masumoto, Y. Indian Ocean warming modulates Pacific climate change. *Proc. Natl Acad. Sci. USA* **109,** 18701–18706 (2012).
31. Ishii, M. & Kimoto, M. Reevaluation of historical ocean heat content variations with time-varying XBT and MBT depth bias corrections. *J. Oceanogr.* **65,** 287–299 (2009).

Acknowledgements

We acknowledge the modelling groups, the Program For Climate Model Diagnosis and Intercomparison (PCMDI) and the Working Group on Coupled Modelling (WGCM) of the World Climate Research Programme (WCRP) for their efforts in making the CMIP5 multi-model data set available. We thank T. Tanaka for running MIROC5.2. This work was supported by Grant-in-Aid 24241009 and the Program for Risk Information on Climate Change (SOUSEI program) from the Ministry of Education, Culture, Sports, Science and Technology (MEXT), Japan.

Author contributions

M.W. designed the study, conducted the numerical experiments, and wrote the paper. C.T. performed the analysis, prepared the figures, and helped write the manuscript.

Additional information

Supplementary information is available in the online version of the paper. Reprints and permissions information is available online at www.nature.com/reprints. Correspondence and requests for materials should be addressed to M.W.

Competing financial interests

The authors declare no competing financial interests.

Methods

Observational data. We used observed monthly SSTs derived from COBE SST during 1845–2014 and a concomitant ocean temperature data set for 1945–2014, both having a 1° horizontal resolution[31]. Surface wind data were derived from the Twentieth Century Reanalysis (20CR) Project[32] for 1871–2012 and the Japanese 55-Year Reanalysis (JRA55) Project[33] for 1958–2014, the latter data set also providing SLP. Monthly precipitation data were based on the Global Precipitation Climatology Project (GPCP)[34].

Model and experiments. We used the Model for Interdisciplinary Research on Climate version 5.2 (MIROC5.2) CGCM (ref. 6), cooperatively developed at the Atmosphere and Ocean Research Institute (AORI) of The University of Tokyo, the National Institute for Environmental Studies (NIES), and the Japan Agency for Marine Earth Science and Technology (JAMSTEC). The resolution is T85 spectral truncation (horizontal spacing of approximately 150 km) and 40 vertical levels for the atmosphere, whereas the resolution is 1° and 63° vertical levels for the ocean. MIROC5.2 has been updated from our CMIP5 model called MIROC5, but the major properties such as the climatological mean states, twentieth-century warming trend, and equilibrium climate sensitivity remained nearly unchanged. This model allows sulfate aerosols to interact with radiation, and calculates the direct, semi-direct and indirect effects[35].

The MIROC5.2 HIST experiment for 1921–2014 was branched off from the official CMIP5 historical experiments[36] and run with the external forcing used for the historical experiment before 2005 and for the Representative Concentration Pathway 4.5 (RCP4.5) run after 2006. Slightly different initial conditions have been adopted in generating the five-member ensemble. Similarly, two attribution experiments (VOLCONST and SO2CONST, five members for each experiment) were conducted, but with sulfate aerosol forcing of either natural volcanic origin or both natural and anthropogenic origins fixed at 1850 levels. The anthropogenic sulfate emission in 1921 was much lower than the emission in recent decades (18% of the 1990 level), so that the choice of this start year would not affect our conclusions. The initial ten years of data were discarded before the analysis.

Statistics. Observational and simulated data were both compiled to annual-mean anomalies relative to the 1961–1990 mean state. When comparing decadal anomalies, we applied a ten-year low-pass filter to the detrended annual-mean fields. The detrending for the entire period greatly reduces the anthropogenic warming signal, but does not affect results of our attribution (Supplementary Fig. 10). To avoid artefact of the low-pass-filtering to the 20-year linear trends, we instead used five-year running means to the detrended annual anomalies for the trend calculation. A statistical test for correlation coefficients and trends was performed by using a two-sided Student's *t*-test with an estimate of the effective sample size for the filtered data. Uncertainty of the observed trend was quantified using the 95% confidence interval[37]. The uncertainty range of the model ensemble-mean values was presented as either the ensemble standard deviation or a percentile assuming a normal distribution.

Attribution analysis. In the CGCM ensemble, externally forced and internally generated components of variability were defined by the ensemble average and deviations from the ensemble mean (Supplementary Fig. 3). In the MIROC5.2 ensembles, contributions from volcanic sulfate aerosols can be isolated by using the differences between HIST and VOLCONST, whereas the difference between SO2CONST and VOLCONST reveals contributions from anthropogenic sulfate aerosols assuming that the impact of each forcing is additive (Table 1). Anomalies in SO2CONST represent internal variability and forced component induced by non-radiative boundary effects such as those due to land-use change and all radiative forcing parameters, except sulfate aerosols. Linear trends of individual components for 1991–2010, their contributions to the total trend, and verification of the additivity assumption have been fully explored (Supplementary Figs 4 and 11–13).

Modes of decadal SST variability. Two dominant modes of decadal SST variability in the tropical Pacific, namely, the IPO and TBV, can be similarly obtained when the EOF domain includes the North and South Pacific. When we include the Atlantic, the TBV appears as EOF1, whereas the IPO follows as EOF2. This swapping of the fractional variance between the two EOFs happens because the TBV has a large signal in the Atlantic (Fig. 1b,d). The two patterns of variability are thus robust and insensitive to the minor change in the analysis domain.

The origin of the two patterns was further explored by using different definitions of SST anomalies in HIST. Assuming that the internal fluctuations could be filtered out by taking the ensemble average, an EOF analysis was performed on the ensemble-mean decadal SST anomalies (Supplementary Fig. 3a). The resultant EOF1, which accounts for 54.7% of the total variance, is very similar to the TBV pattern shown in Fig. 1d, thus strengthening the argument that the model's TBV is, in the main, a forced variability. Conversely, the HIST ensemble deviation's EOF1, which accounts for 49.0% of the total variance (Supplementary Fig. 3b), resembles the model's IPO pattern (Fig. 1c), indicating that the latter was independent of external forcing. Furthermore, an EOF analysis of a long pre-industrial control simulation (Supplementary Fig. 3c) shows a leading EOF pattern nearly identical to Fig. 1c. The findings are therefore robust in that the IPO pattern emerges as the dominant mode of natural decadal SST variability in the Pacific, which is consistent with previous studies[3,14].

Trends and multidecadal variability in ocean temperature. The importance of aerosols as the primary driver of the Atlantic multidecadal variability (AMV)[19] has been questioned because of a discrepancy in ocean interior temperature changes between model and observation[24]. To strengthen the credibility of our simulations, we examined the Atlantic basin SST (averaged in 0°–70° N and longitudes of 80° W–0°), often called the AMV index[38], and the 0–700 m ocean heat content (HC_{700}) in the North Atlantic (Supplementary Fig. 5). The AMV indices in observations and the HIST ensemble mean show a multidecadal variability imposed on a linear trend, and the detrended time series are significantly correlated ($r = 0.73$). The multidecadal variability in SO2CONST is weak, and not significantly correlated with observations. A greater reproducibility of HC_{700} is also seen in HIST, showing an increasing trend similar to the observations for 1945–2014. The long-term trend is over-represented in SO2CONST, which furthermore lacks multidecadal variations. Therefore, the failure to capture the observed heat content change in the previous model study[19], linking aerosols to the AMV, is not observed in the MIROC5.2 simulations.

Because the aerosol radiative effect is subject to uncertainty in GCMs[39], the relevance of the sulfate aerosol forcing in HIST is confirmed by the global-mean surface air temperature (SAT) time series compared with observations of HadCRUT4 (ref. 40) (Supplementary Fig. 8). Except for discrepancies around 1940 and after 2000, the latter known as the failure of simulating the global warming hiatus[4–6], the SAT time series in the HIST ensemble mean is in good agreement with the observations, including the linear trend for 1931–2014 and the cooling response to the Pinatubo eruption. In SO2CONST, the warming trend is 1.4 times larger than that of HIST owing to the lack of sulfate aerosol cooling, and furthermore, its multidecadal variability is very weak.

The long-term linear detrending greatly reduces the anthropogenic warming signal, but it does not affect the results of the present study. This is confirmed by the 10-year low-pass SST anomalies in the WNP, without long-term detrending, in observations, HIST, and SO2CONST (Supplementary Fig. 10). The 1991–2010 warming trends in observations and HIST were clearly not seen in the past decades, whereas the warming trend in SO2CONST is similar to the linear trend during 1931–2014.

Mechanism of the decadal SST variability associated with the TBV. The extent to which aerosol radiative forcing could account for the local correlation between observed and simulated decadal SST anomalies (Fig. 2a) was examined using surface energy budgets. Because sulfate aerosols affect SST through the modulation of surface shortwave radiation (SW_{sfc})[19–22], we expect to find a positive correlation between decadal SST and SW_{sfc} anomalies where the time-varying aerosol concentration locally drives the SST variability.

In reality, a significant positive correlation between these variables was found in the tropical Atlantic ($r = 0.89$), but not in the western Pacific (Supplementary Fig. 6a). Although the clear-sky SW_{sfc} that measures the aerosol direct effect[23] is positively correlated with the SST anomaly in the WNP, the cloud SW_{sfc} that represents the aerosol indirect effect interferes, leading to a weak correlation ($r = 0.25$) between the decadal SST and net SW_{sfc} anomalies in the WNP (Supplementary Fig. 6b,c). However, decadal SST anomalies in the WNP are significantly and positively correlated with the decadal latent heat flux anomalies (Supplementary Fig. 6d). This is in contrast to the other regions, including the tropical Atlantic, where latent heat flux anomalies are negatively correlated with the SST anomalies; this is indicative of an evaporative damping effect on the SST variability. Overall, sulfate aerosol forcing was locally active in the tropical Atlantic, where it generated multidecadal SST variability, whereas the coherent SST variability in the WNP was not directly due to aerosol forcing; instead, it was induced dynamically by the tropical circulation changes. This remote mechanism originating in the tropical Atlantic appears consistent with previous modelling studies demonstrating the Atlantic impact on the Pacific[9–11,41].

Observed and simulated SST trends over the past two decades. The patterns of SST trends for 1991–2010 in observations and HIST (Fig. 3a,b)—albeit they are different in the central-eastern tropical Pacific—can both be explained by a combination of trends in the IPO and the TBV. This was demonstrated by reconstructing the decadal SST anomaly fields by using two EOFs (Supplementary Fig. 7a,d). Because each EOF is orthogonal, the reconstructed SST trends are divided into two trend patterns associated with the respective EOF. In the observations, the central-eastern Pacific cooling trend can be explained by the negative trend in the IPO, whereas the western Pacific warming is due to the positive TBV trend (Supplementary Fig. 7b,c). A large discrepancy between

observations and HIST is the lack of a cooling trend associated with the IPO (Supplementary Fig. 7e). This is not surprising, given that the internally generated IPO has various phases across the ensemble members. Consequently, the contribution of the TBV to the SST trend for 1991–2010, as measured by the fraction of the trend pattern explained by EOF2, is much larger in the simulation; about 40% and 83% for observations and HIST, respectively.

Decomposition of the HIST ensemble mean using the three ensembles. The contributions of volcanic and anthropogenic sulfate aerosols to the WNP SST trends were estimated using a combination of the three sets of ensemble-mean anomalies (Table 1). Here, those components are re-defined not only for the WNP SST, but also for other fields for further attribution analysis:

ALL = HIST,
AERO = HIST − SO2CONST,
ANTH = VOLCONST − SO2CONST,
VOLC = HIST − VOLCONST,
OTHER = SO2CONST,

where the left-hand side denotes the name of the component and the right-hand side indicates the name of the experiment. By definition, ALL is decomposed into ALL = AERO + OTHER, and AERO is equal to ANTH + VOLC. Shown in Supplementary Fig. 4a,b are local correlation maps of the decadal SST anomalies between observations and the above two components—that is, OTHER and AERO—indicating the dominant role of sulfate aerosol forcing in the decadal/multidecadal variability in the WNP and the Atlantic SSTs (red and blue box regions).

The patterns of the 1991–2010 trend in the HIST ensemble mean (Fig. 3b,d) are decomposed into the above components (Supplementary Fig. 11). It is clear (and consistent with the results in Table 1) that AERO shows fairly similar patterns to ALL (=HIST), which is further explained the most by VOLC. The intensification of trade winds in ALL and AERO is associated with ascending and descending trends in the vertical velocity in the western and central equatorial Pacific (Supplementary Fig. 12). Although an aerosol-induced easterly trend in the western Pacific has been obtained in a previous study[22], the overall patterns of the circulation trends are different, plausibly owing to different periods for the trend.

Using a 20-year sliding window (see Fig. 4d–f), the fractional contributions of each component to ALL in the WNP SST trend is estimated for the entire period (Supplementary Fig. 13). The values for 2010 in Supplementary Fig. 13b are shown in Table 1. Again, it is evident that AERO reproduces most of the trends in ALL (black and orange curves in Supplementary Fig. 13a). However, the relative contribution of volcanic and anthropogenic aerosols varies in time, and shows a comparable contribution in the 1980s and 1990s, whereas the volcanic contribution dominates in the recent two decades and in the middle of the twentieth century (Supplementary Fig. 13b).

Additivity of aerosol and other radiative forcings. We have defined the decadal anomalies forced by sulfate aerosols using AERO, assuming that the forced components are additive. This assumption was tested by performing an additional five-member ensemble experiment, called SO2ONLY. This experiment is the same as HIST, but all the external radiative forcing agents except for volcanic and anthropogenic sulfate aerosols have been fixed at the 1850 level. The ensemble-mean anomalies can be directly compared between AERO and SO2ONLY (Supplementary Fig. 4b–e). It is remarkable that the spatial patterns of local correlation of the decadal SST anomalies with observations are similar to each other in the two ensembles. Moreover, the time series of the WNP SST anomalies both show a significant increasing trend for 1991–2010 (0.15 ± 0.15 and 0.16 ± 0.08 °C per decade, respectively). The above result clearly shows that the additivity assumption of aerosol forcing was appropriate for the multidecadal SST variability investigated in the present study.

CMIP5 models and analysis. Combined data from historical and RCP4.5 experiments were used for the following 26 CGCMs (single member for each model): ACCESS1.0, ACCESS1.3, BCC-CSM1.1, BCC-CSM1.1-M, CanESM2, CMCC-CM, CMCC-CMS, CNRM-CM5, CSIRO-Mk3.6.0, GFDL-CM3, GFDL-ESM2G, GFDL-ESM2M, GISS-E2-H, GISS-E2-R, HadGEM2-CC, HadGEM2-ES, INM-CM4, IPSL-CM5A-LR, IPSL-CM5A-MR, IPSL-CM5B-LR, MIROC5, MIROC-ESM, MPI-ESM-LR, MPI-ESM-MR, MRI-CGCM3 and NorESM1-M. Some of the models do not incorporate the aerosol indirect radiative effect, but the multi-model mean trends were not significantly different when we selected a subset of models that include both direct and first-order indirect effects of sulfate aerosols by referring to previous studies[42–44]. It turned out that the multi-model mean trends in the WNP and the Atlantic SST anomalies for 1991–2010 are significantly positive as in MIROC5.2, but the values (0.17 ± 0.1 and 0.18 ± 0.09 °C per decade) account only for 74–86% of the trends in the HIST ensemble mean (Supplementary Fig. 9a–c). This suggests that some models failed to capture the recent warming in these regions. Similarly, the multi-model mean surface easterly is accelerated in the central Pacific, but with a much weaker magnitude than HIST (Supplementary Fig. 9a,d).

References

32. Compo, G. P. *et al*. The Twentieth Century Reanalysis project. *Q. J. R. Meteorol. Soc.* **137,** 1–28 (2011).
33. Kobayashi, S. *et al*. The JRA-55 reanalysis: general specifications and basic characteristics. *J. Meteorol. Soc. Japan* **93,** 5–48 (2015).
34. Adler, R. F. *et al*. The version 2 global precipitation climatology project (GPCP) monthly precipitation analysis (1979–Present). *J. Hydrometeorol.* **4,** 1147–1167 (2003).
35. Takemura, T. *et al*. A simulation of the global distribution and radiative forcing of soil dust aerosols at the Last Glacial Maximum. *Atmos. Chem. Phys.* **9,** 3061–3073 (2009).
36. Taylor, K. E., Stouffer, R. J. & Meehl, G. A. An overview of CMIP5 and the experiment design. *Bull. Am. Meteorol. Soc.* **93,** 485–498 (2011).
37. Santer, B. D. *et al*. Statistical significance of trends and trend differences in layer-average atmospheric temperature time series. *J. Geophys. Res.* **105,** 7337–7356 (2000).
38. Mahajan, S., Zhang, R. & Delworth, T. Impact of the Atlantic Meridional Overturning Circulation (AMOC) on Arctic surface air temperature and sea ice variability. *J. Clim.* **24,** 6573–6581 (2011).
39. Cherian, R., Quaas, J., Salzmann, M. & Wild, M. Pollution trends over Europe constrain global aerosol forcing as simulated by climate models. *Geophys. Res. Lett.* **41,** 2176–2181 (2014).
40. Morice, C. P., Kennedy, J. J., Rayner, N. A. & Jones, P. D. Quantifying uncertainties in global and regional temperature change using an ensemble of observational estimates: the HadCRUT4 dataset. *J. Geophys. Res.* **117,** D08101 (2012).
41. Kucharski, F. I. S., Kang, R. F. & Laura, F. Tropical Pacific response to 20th century Atlantic warming. *Geophys. Res. Lett.* **38,** L03702 (2011).
42. Wilcox, L. J., Highwood, E. J. & Dunstone, N. J. The influence of anthropogenic aerosol on multi-decadal variations of historical global climate. *Environ. Res. Lett.* **8,** 024033 (2013).
43. Allen, R. J. A 21st century northward tropical precipitation shift caused by future anthropogenic aerosol reductions. *J. Geophys. Res.* **120,** 9087–9102 (2015).
44. Rotstayn, L. D., Collier, M. A., Shindell, D. T. & Boucher, O. Why does aerosol forcing control historical global-mean surface temperature change in CMIP5 models? *J. Clim.* **28,** 6608–6625 (2015).